Controlled gel expansion through colloid oscillation

Guido L. A. Kusters,[1,*] Cornelis Storm,[1,2] and Paul van der Schoot[1]
[1]*Department of Applied Physics, Eindhoven University of Technology, PO Box 513, 5600 MB Eindhoven, The Netherlands*
[2]*Institute for Complex Molecular Systems, Eindhoven University of Technology, PO Box 513, 5600 MB Eindhoven, The Netherlands*

(Received 29 July 2022; accepted 11 October 2022; published 28 October 2022)

We model the behavior of a single colloid embedded in a cross-linked polymer gel, immersed in a viscous background fluid. External fields actuate the particle into a periodic motion, which deforms the embedding matrix and creates a local microcavity, containing the particle and any free volume created by its motion. This cavity exists only as long as the particle is actuated and, when present, reduces the local density of the material, leading to swelling. We show that the model exhibits rich resonance features, but is overall characterized by clear scaling laws at low and high driving frequencies, and a pronounced resonance at intermediate frequencies. Our model predictions suggest that both the magnitude and position of the resonance can be varied by varying the material's elastic modulus or cross-linking density, whereas the local viscosity primarily has a dampening effect. Our work implies appreciable free-volume generation is possible by dispersing a collection of colloids in the medium, even at the level of a simple superposition approximation.

DOI: 10.1103/PhysRevE.106.044609

I. INTRODUCTION

In nature there are many examples of biological systems that must adapt to their environment to maintain functionality, ranging from the intra- and intercellular signaling of proteins [1], to the directed motion, e.g., chemotaxis, of bacteria [2], and the tailored seed dispersal strategies of plants [3,4]. With the envisioned goal of replicating such functionality in mind, scientific research into artificial, stimuli-responsive materials has enjoyed significant interest in recent years [5–8]. Generally, this concerns systems comprising synthetic polymers that respond suitably to, for example, a variation of the pH or temperature [9,10], the application of an electric or magnetic field [11,12], or the irradiation of light with a suitable wavelength or intensity [13,14]. Prospective applications include on-demand drug delivery [15,16], tissue (re)generation [17,18], and artificial muscles [19–21].

The physical properties that must be suitably altered for such applications include, but are not limited to, the porosity [22], conformation [23], wettability [24], and adhesion [25] of the material. This response is typically programed into the material on the molecular scale, during the synthesis [5–8]. Although this enables fine control over the resulting behavior, it also limits the pool of suitable material candidates. In this paper, we explore an alternative approach, which can render *any* cross-linked polymer network, immersed in a viscoelastic background fluid, responsive in a controlled manner.

To this end, we propose embedding responsive colloids into the gel. Upon subsequent stimulation with an oscillatory external field, e.g., electric or magnetic, we expect the colloids to create microscopic cavities by displacing the embedding matrix during their oscillation. The generated free volume (locally) reduces the density of the material and, in doing so, increases its porosity.

Although the concept of embedding responsive colloids into a polymer network is not necessarily new [26–28], its application to volume expansion and porosity is. Nevertheless, there is some precedent for the underlying mechanism. For example, Sozanski and coworkers recently conducted viscosity experiments on aqueous solutions of polyethelene glycol using a quartz tuning fork, oscillating at nanoscopic amplitudes [29]. For semidilute solutions of high molecular weight, they report a significant drop in the local viscosity, orders of magnitude below that of the bulk, which they rationalize based on the motion of a dynamic depletion layer, i.e., a region of free volume.

In addition, the working mechanism we propose is reminiscent of that utilized in liquid-crystalline networks, where rod-like mesogens are embedded in a dense polymer network [30]. For applications, these mesogens are usually functionalized with either a strong dipole moment [31] or an azobenzene moiety [32,33]. In the former case, application of an alternating electric field induces mesogen reorientation, whereas in the latter case exposure to irradiation of a suitable wavelength induces trans-to-cis interconversion. Both are known to result in the generation of free volume [31,32]. Similar to the above materials, we envision our approach contributing to the realization of self-cleaning properties [34], pattern formation [35–39], and transport of molecular cargo [40,41].

To achieve such functionality in a controlled manner, theoretical insight into the underlying mechanism of volume generation is required. To achieve this, we take inspiration from the field of active microrheology [42], which likewise studies the driven motion of a colloid immersed in a viscoelastic environment albeit in a noninvasive manner. Since the pioneering work of Batchelor [43–45], theoretical efforts have primarily focused on relating the interactions between a

*g.l.a.kusters@tue.nl

"probe" colloid and the local microstructure to global material properties [46–50]. In addition, the motion of the "probe" particle itself, as it is driven through the polymer environment, has also been studied extensively, where particular focus has been given to the role of hydrodynamics [51,52], depletion interactions [53–56], and viscosity [57]. Notwithstanding these important contributions, our focus is instead on how the motion of such a colloid can *perturb* the local microstructure. We use a considerably simpler model in the form of a driven harmonic oscillator, extended to reflect its coupling to the viscoelastic environment, i.e., the cross-linked polymer gel with viscous background fluid, into which the colloid is embedded.

We detail our theoretical model, based on a generalized harmonic oscillator, in Secs. II-III. Following this, in Sec. IV, we characterize the oscillation of the colloid by reporting the amplitude as a function of the driving frequency. We show numerically that the model exhibits clear scaling laws in the low- and high-frequency limits, and a resonance at intermediate driving frequencies. These can all be calculated reasonably accurately by making simplifying assumptions. Next, in Sec. V, we link the colloid oscillation to volume expansion by investigating the steady-state cavity volume. For this we likewise derive clear scaling laws and locate a distinct resonance that suggests volume expansion far exceeding the length scale of the colloid is possible. Subsequently, in Sec. VI, we investigate the effect of varying both the elasticity of the polymer network, accessible via the gel's elastic modulus or cross-linking density, and the viscosity of the background fluid. The former shifts both the position and the magnitude of the resonance, whereas the latter mainly has a dampening effect. Finally, we conclude by summarising our most salient results and reflecting on their significance in view of experiments, in Sec. VII.

II. THEORETICAL MODEL

We model the motion of a colloid embedded in a cross-linked polymer gel, which is in turn immersed in a viscous background fluid, by means of a generalized, driven harmonic oscillator. As point of departure, we consider a colloid of mass m and diameter $2a$, which we assume is greater than the distance between permanent crosslinks in the gel. The colloid is driven through a viscoelastic environment that is characterized by an elastic spring constant k and a viscous damping coefficient c. For a gel, the latter is directly related to the viscosity of the background fluid. Assuming a driving force of magnitude F_0 and driving frequency ω, the resulting equation of motion for the colloid position $x = x(t)$ reads

$$m\ddot{x} + c\dot{x} + kx = F_0 \sin \omega t, \tag{1}$$

where dots indicate derivatives with respect to time t. Note that in writing Eq. (1), we assume Stokes-like drag with the viscous background fluid, neglecting potential temperature-driven diffusive motion. This is justified in the limit of dense, cross-linked polymer networks, in which the motion of the colloid is dominated by the external driving force and the resisting polymer network. For the remainder of this paper, we focus on this limit and assume that, initially, the colloid is at rest and there is no residual stress in the network.

The philosophy of the model is that the colloid, through its oscillatory motion, creates a microscopic cavity, containing itself and the viscous background fluid, by displacing polymeric material. Figure 1 schematically shows this process. From the first two panels, we see that, as the external field is applied, the colloid perturbs the polymer network from its initial, stress-free configuration by locally compressing it. This compression is resisted by an elastic restoring force, and the cavity that opens up in the wake of the colloid relaxes viscoelastically. The third panel coincides approximately with the change in sign of the oscillatory external field, marking the turning point of the oscillation. Here, the elastic restoring force, which is now directed parallel to the colloid velocity, still applies and the viscoelastic relaxation of the cavity likewise continues. Following this, the fourth panel illustrates that if the colloid separates from the cavity wall, no elastic force acts on it, and both cavity walls relax viscoelastically. Finally, the bottom panels show how the oscillation continues as the colloid makes contact with the opposite cavity wall, and the same steps are repeated. The colloid experiences friction with the viscous background fluid at all of these stages.

For the sake of simplicity, we have tacitly assumed that the polymer network does not screen the viscous friction of the colloid with the background fluid in writing the above, such that only the elastic force depends on whether the colloid makes contact with the cavity wall. This transforms Eq. (1) into

$$m\ddot{x} + c\dot{x} + kx\,\delta_{\text{contact}} = F_0 \sin \omega t, \tag{2}$$

where we have introduced the "contact function," δ_{contact}, which is unity if the colloid is in contact with a cavity wall and zero otherwise (see Fig. 1). Note that our qualitative results in this paper are robust even upon relaxing the assumption of no screening, which we explore in Appendix A.

The above makes clear that physical contact between the colloid and cavity wall is a crucial aspect of the model. However, to realize its consistent implementation, we must make a choice regarding the equilibrium configuration the polymer network relaxes toward. Is all relaxation in our one-dimensional description purely elastic, with any given cavity wall only relaxing as far as its initial position, or can plastic rearrangements also occur, where the cavity wall relaxes beyond its initial position to fill the microscopic cavity? In this paper, we pursue the latter choice, as we intuitively expect a unilateral displacement of the colloid to not give rise to any *lasting* free volume. In addition, if we were to for the moment consider the free-volume generation from a three-dimensional perspective, not only the cavity walls but also the sides of the cavity play a role. That is, even if the noncompressed cavity wall is under no stress, the sides of the cavity experience extensional stresses that promote locally shrinking the cross section of the cavity. Translated to our one-dimensional picture, this again results in a relaxation of the cavity wall that effectively goes beyond its initial position. Thus, in what follows, we assume that the microscopic cavity relaxes viscoelastically until it fully collapses. Further below we explain how we model this.

However, we first address a complication this choice carries with it. Namely, if the cavity wall is allowed to relax beyond its initial position via plastic rearrangements, we must

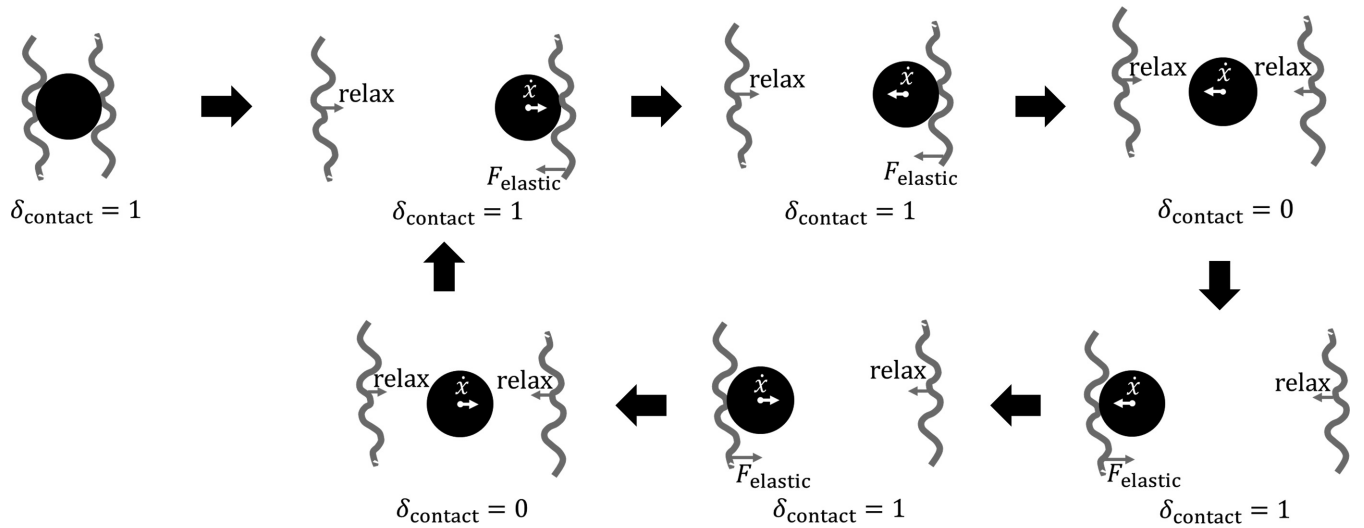

FIG. 1. Schematic illustration of the colloid oscillation, including the direction of the velocity, forces, and polymer relaxation. The significance of the functions δ_{contact}, discussed in the main text, is also illustrated.

give careful thought to the rest position of the elastic force, $x_{0,\text{wall}}(t)$, and how it evolves with time; this rest position is generally different for the different cavity walls, meaning $x_{0,\text{left}}(t) \neq x_{0,\text{right}}(t)$. We cannot simply set $x_{0,\text{wall}}(t) = 0$, since if the cavity wall in question relaxes beyond its initial position $x = 0$, it would then not resist but instead accelerate the motion of the colloid upon contact. Equating the rest position, $x_{0,\text{wall}}(t)$, with the colloid position, $x(t)$, at any time that contact is established leads to different complications. This approach would artificially and progressively weaken the network in the case the external field repeatedly pushes the colloid into the polymer network, which in turn rebuffs it; this is a scenario we encounter in our numerical evaluation of the model.

We reconcile the above concerns by, upon establishing contact between colloid and cavity wall, *only* equating the rest position with the colloid position if the colloid has moved beyond the current rest position, i.e., if $x(t) > x_{0,\text{left}}(t)$ or $x(t) < x_{0,\text{right}}(t)$. In essence, this means we assume relaxation is effectively elastic until the cavity wall reaches its current rest position. Beyond this point, relaxation occurs via plastic rearrangements and thus continually increases the rest position, until the cavity wall is again perturbed by the colloid. We carry out this procedure separately for both cavity walls. With this in mind, Eq. (2) becomes

$$m\ddot{x} + c\dot{x} + k(x - x_{0,\text{wall}})\delta_{\text{contact}} = F_0 \sin \omega t, \tag{3}$$

where $x_{0,\text{wall}} = x_{0,\text{wall}}(t)$ depends crucially on the cavity wall with which the colloid is in contact and the deformation history of the network. A consequence of this choice is that inversion symmetry along the x-axis is broken: applying an external field $\propto \pm \sin \omega t$ yields identical oscillations, but mirrored in $x = 0$. Thus, within this set of assumptions, the transient stages of dynamics can have a lasting effect on the eventual steady state that is reached: a direct consequence of the occurrence plastic rearrangements. This we shall see when we discuss our results in Sec. IV.

Finally, we link the colloid dynamics to that of the microscopic cavity by specifying the evolution of the cavity volume. To this end, we propose that the colloid creates a tubular cavity, with a cross section equal to that of the colloid, during its oscillation. The corresponding increase in cavity free volume v, i.e., the volume of the cavity in excess of the colloid volume, then reads

$$\dot{v} = |\dot{x}|\pi a^2 \, \delta_{\text{contact}} - \frac{v}{t_R}, \tag{4}$$

where the first term, representing expansion, only applies if the colloid is in contact with the polymer network. The absolute sign implies that variation in cavity free volume occurs at double the frequency of the colloid oscillation, as free volume is generated upon both leftward and rightward motion. The second term describes the relaxation of the microscopic cavity, with t_R the typical relaxation time of the cross-linked polymer gel. The underlying assumption here is one of Rouse-like relaxation, where we take the dynamics to be dominated by the lowest-order mode [58]. That is, we assume the slowest mode that can be excited is on the order of the distance between permanent crosslinks, which we associate with the relaxation time t_R, and we neglect modes on shorter length scales, which relax significantly faster. Looking ahead, relaxation of deformations on longer length scales, such as for relaxation of the bulk, can still occur on longer timescales. However, as we shall see below, the system eventually achieves a steady state oscillation, such that, if given enough time, the bulk can invariably adjust to any local changes in density effected by the colloid.

This concludes the discussion of our theoretical model. Before we investigate the resulting model dynamics, we first scale the theory to make it dimensionless, reducing the number of variable parameters.

III. SCALING PROCEDURE

To scale Eqs. (3) and (4), we take t_R as the typical timescale of the host material, and identify $L = F_0 {t_R}^2/m$ as its typical length scale. This quantity is physically related to the distance a force of magnitude F_0 would pull the colloid of mass m in the

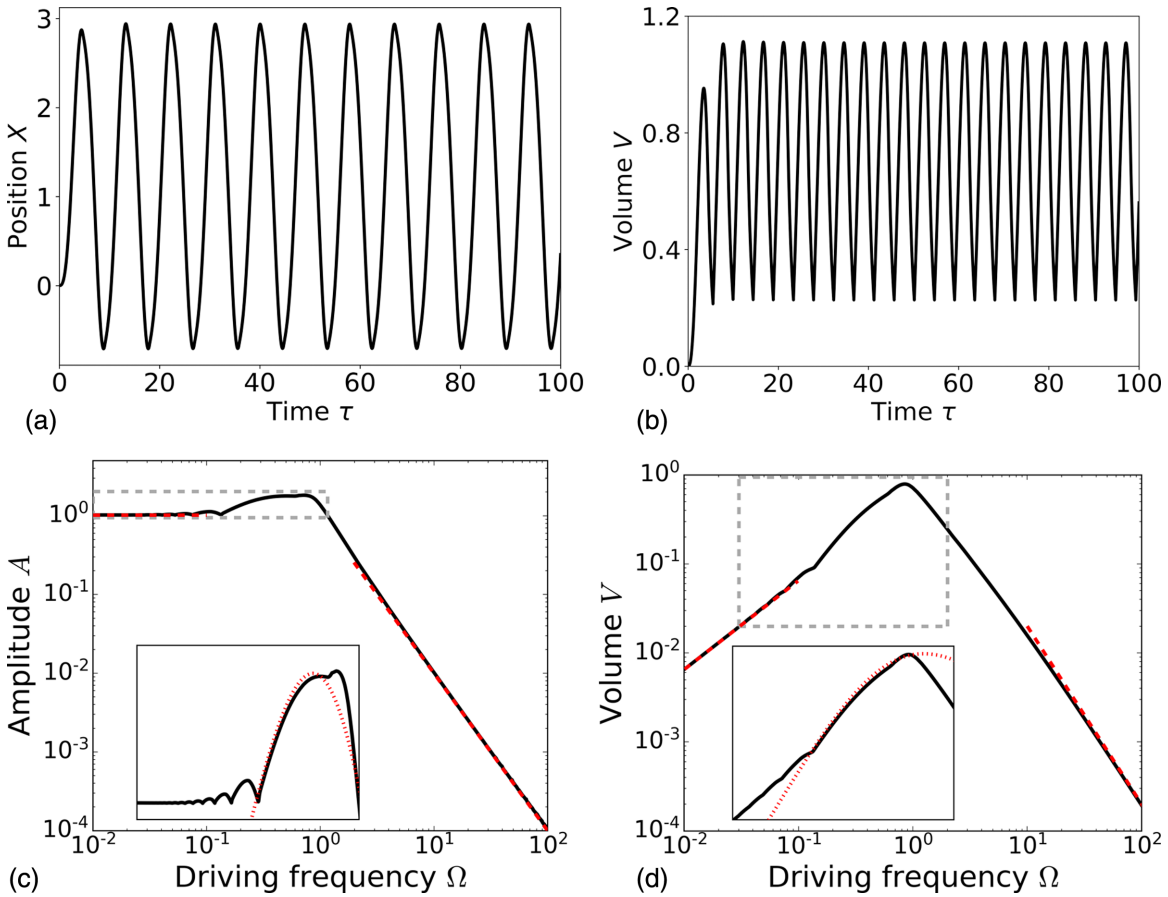

FIG. 2. (Top) Scaled colloid position X (left) and the cavity volume V (right) as a function of the scaled time τ, corresponding to the scaled driving frequency $\Omega = \Omega_0/\sqrt{1-2B^2/\Omega_0^2}$. (Bottom) Scaled steady-state amplitude A of the colloid oscillation (left) and the corresponding cavity volume V (right) as a function of the scaled driving frequency Ω, on a logarithmic scale. The dashed red lines denote the low- and high-frequency scaling laws $A_{\text{low}} = 1/2\Omega_0^2$ and $V_{\text{low}} = \Omega/\pi\Omega_0^2$, and $A_{\text{high}} = 1/\Omega^2$ and $V_{\text{high}} = 2/\Omega^2$, respectively. The zoomed-in inset is indicated in grey; the dotted red curves in the insets correspond to the theoretical estimates of Eq. (7) (left) and Eq. (8) (right), respectively. Parameter values used: $\Omega_0 = 0.7$, $B = 0.05$.

relaxation time t_R, if we disregard the embedding matrix and background fluid. Subsequently introducing the scaled time, $\tau = t/t_R$, the scaled colloid position, $X = x/L$, and the scaled cavity volume, $V = v/L\pi a^2$, the set of scaled governing equations becomes

$$\begin{cases} \ddot{X} + 2B\dot{X} + \Omega_0^2(X - X_0)\delta_{\text{contact}} = \sin\Omega\tau, \\ \dot{V} = |\dot{X}|\,\delta_{\text{contact}} - V. \end{cases} \tag{5}$$

Here, the derivatives are taken with respect to the scaled time, and we have expressed the model in terms of the scaled quantities

$$\begin{cases} B = \frac{ct_R}{2m}, \\ \Omega_0 = \sqrt{\frac{k}{m}}t_R, \\ \Omega = \omega t_R. \end{cases} \tag{6}$$

The above procedure reduces the number of model parameters to two: the scaled damping ratio, B, and the scaled natural frequency of the oscillator, Ω_0. The most straightforward experimental link to the former is through the viscosity of the background fluid, whereas the latter depends strongly on the gel's elastic modulus and its cross-link density. Also implicit in the scaling is that our results can be tuned by varying the mass and radius of the colloid, the relaxation time of the gel, and the magnitude of the external driving force. The above allows us to comprehensively scan the parameter space and numerically find the steady-state solutions for a given scaled driving frequency Ω. This we do by means of a standard fourth-order Runge-Kutta scheme, adapted to account for the contact function we use.

This establishes the scaled model we use for the remainder of this paper. In order to provide an overview of the dynamical response it gives rise to, we now present the ensuing colloid dynamics for a range of driving frequencies.

IV. COLLOID DYNAMICS

Figure 2(a) shows a typical oscillation of the colloid position, corresponding to a driving frequency $\Omega = \Omega_0/\sqrt{1-2B^2/\Omega_0^2}$. This is the resonant frequency of the "bare" harmonic oscillator, in the absence of the changes we introduced to model the viscous cavity. From the figure we see that, unlike what is expected for a simple harmonic oscillator, the colloid traces out a trajectory that is asymmetric about the origin. As foreshadowed, this is a direct consequence of

allowing plastic rearrangements within the model, as opposed to purely elastic deformations. Since which plastic rearrangements occur is largely determined during the transient stages of dynamics, the initial form of the external field matters for the eventual steady state that is reached.

This also explains why we deliberately choose to apply a sine function as the external field, rather than a cosine. The initial "kick" provided by the latter would immediately induce plastic rearrangements, which in turn affect the steady state. This presents a counter-intuitive prediction—the distinctness of the steady-state oscillations driven by sine and cosine fields, especially at low frequencies—that could be straightforwardly verified through experiments. In Appendix D, we work out the corresponding differences and their origins, which we expect to become more important for more densely packed and cross-linked polymer networks. In this paper, however, we shall err on the side of caution by focusing on external fields that initially vary slowly, so as to prevent possibly spurious plastic rearrangements. We return to this point at the end of Sec. VII.

To investigate the dynamics of the colloid from a broader perspective, Fig. 2(c) shows the scaled steady-state oscillation amplitude of the colloid, A, as a function of the driving frequency of the external field, Ω. From this we primarily conclude that the model obeys clear scaling laws in the low- and high-frequency limits, as indicated by the dashed red lines. In between these limits, at intermediate driving frequencies, we find a pronounced resonance. This is clarified by the zoomed-in inset, the boundaries of which are indicated by the dashed grey lines. Here, the dotted red line represents a theoretical estimate, which we shall discuss further below [see Eq. (7)]. Finally, the model also exhibits a host of finer features, including the resonance peak being split in two and the emergence of multiple local optima in the low-frequency regime. These features add to the depth of our model but are not crucial to our message in this paper, hence we discuss them in Appendix B.

We commence by rationalising the amplitude in the low-frequency limit, where we expect only the elastic and driving force in Eq. (5) to contribute meaningfully to the dynamics. As a result, the two should balance at the turning point of the oscillation, where $\sin\Omega\tau = 1$, yielding $A_{\text{low}} = 1/2\Omega_0^2$ (dashed red line). From the figure it is apparent there is good agreement with the numerical results (black curve). Conversely, we expect the high-frequency limit to reflect a competition between the inertial term and the driving force. Equating the two and Fourier transforming the result shows that steady-state solutions must take the form $X(\tau) = \sin\Omega\tau/\Omega^2$, which likewise agrees with the scaling law $A_{\text{high}} = 1/\Omega^2$ shown in the figure (dashed red line).

Although neither of the above lines of reasoning translates perfectly to intermediate driving frequencies, here we can make headway by neglecting viscous friction and presuming that the colloid maintains contact with the cavity wall until reaching its turning point. This is reasonable for systems dominated by elastic rather than viscous effects. If we furthermore presume that the colloid leaves this turning point with no significant residual velocity or acceleration, it follows the same trajectory back to its starting position, from which the oscillation continues identically. Under these assumptions, the entire oscillation is effectively determined upon reaching the first turning point, suggesting that its amplitude can be deduced by computing said turning point. This we do by setting $\delta_{\text{contact}} = 1$ and $B = 0 = X_0$ in Eq. (5), which yields

$$A_{\text{intermediate}} = \frac{1}{2}\frac{\Omega\sin\left(\frac{2\pi\Omega_0}{\Omega+\Omega_0}\right) - \Omega_0\sin\left(\frac{2\pi\Omega}{\Omega+\Omega_0}\right)}{\Omega^2\Omega_0 - \Omega_0^3}. \tag{7}$$

This equation is plotted as a dotted red line in the inset of Fig. 2(c), from which good agreement with the numerical results is apparent for the modest values of Ω_0 and B used here. Below, in Sec. V, we derive a similar equation for the concomitantly generated free volume V.

The above estimate and scaling relations capture the overall response of the colloid to the external field. Below, in Sec. V, we discuss the overall cavity volume the colloid oscillation gives rise to in the steady state.

V. CAVITY EXPANSION

Figure 2(b) shows the cavity free volume, i.e., the cavity volume in excess of the colloid volume, resulting from the colloid oscillation shown in Fig. 2(a). The frequency of this curve is twice as high as that of the colloid oscillation, since free volume is generated upon both leftward and rightward motion. In addition, the asymmetry between the bottom (sharp) and the top (rounded) of the curve can be traced back to free volume generation being tied directly to the colloid making contact with the cavity wall.

To investigate how we might influence the cavity dynamics through our choice of external actuation, Fig. 2(d) shows the steady-state cavity free volume for a range of driving frequencies. The figure is closely related to the steady-state oscillation amplitude shown in Fig. 2(c), which can be interpreted as an upper bound for free volume generation. The actual free volume is lower due to the viscoelastic relaxation of the gel.

As before, the model exhibits distinct scaling laws in the low- and high-frequency limits, indicated by the dashed red lines. Here, the low-frequency behavior is markedly different from that of the oscillation amplitude [Fig. 2(c)] due to the aforementioned relaxation, tending to zero in the low-frequency limit. The zoomed-in inset shown in the figure again highlights the resonance of the system, where the dotted red curve denotes a theoretical estimate to which we shall return further below [see Eq. (8) below]. We discuss the finer features of the model in Appendix C.

Notably, Fig. 2(d) communicates that a steady-state expansion of up to $V \approx 1$, as measured on the system's natural length scale L, can be achieved. We argue that this constitutes a significant expansion, which we support by means of a rough estimate. If we assume a homogeneous, spherical gold nanoparticle with a radius of $a = 25\,\text{nm}$ and a surface charge density of $-2\,\text{mC}$ [59], subject to an electric field with strength $1\,\text{V/m}$ and immersed in a polystyrene network with Rouse time $t_R = 1\,\text{cs}$ [60], we find that the system's typical length scale equals $L \approx 1\,\text{mm}$. Given that the resonance peak shown in Fig. 2(d) obeys $V \approx 1$, measured on this length scale, we conclude that volume increases far exceeding the length scale of the colloid are in principle possible.

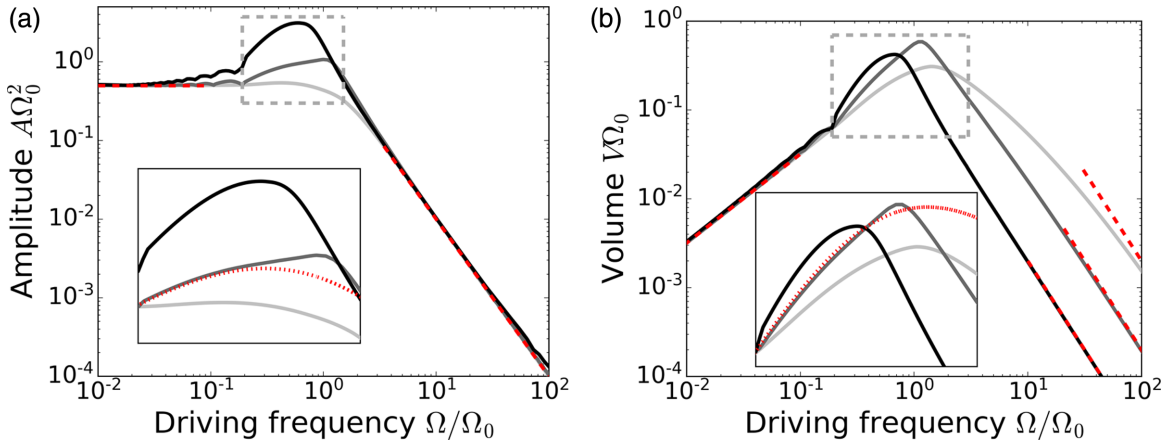

FIG. 3. Scaled steady-state amplitude, A, of the colloid oscillation (left) and the corresponding cavity free volume V (right) as a function of the scaled driving frequency Ω, on logarithmic scale. The curves correspond to $\Omega_0 = 0.1$ (silver), 1.0 (grey), and 10.0 (black), all for $B = 0.05$. The dashed red lines denote low- and high-frequency scaling laws. The zoomed-in inset is indicated in grey; the dotted red curves in the insets correspond to the theoretical estimates of Eq. (7) (left) and Eq. (8) (right), respectively.

Next, we validate the model through scaling relations in the low- and high-frequency limits. For low driving frequencies, we expect that the colloid is continually pushing against the cavity walls, and that in the steady state the concomitant expansion is compensated exactly by the viscoelastic relaxation of the gel [see Eq. (5)]. Thus estimating the average velocity of the colloid as $(1/\Omega_0^2)/(\pi/\Omega)$ by using the low-frequency estimate of the oscillation amplitude, we find $V_{\text{low}} = \Omega/\pi\Omega_0^2$, as indicated by the left-most dashed red line in Fig. 2(d).

Conversely, for high driving frequencies we expect that the cavity walls have no time to relax, suggesting that in the steady state the extent of the cavity equals twice the oscillation amplitude, $V_{\text{high}} = 2/\Omega^2$. This is shown by the right-most dashed red line in Fig. 2(d), which again demonstrates good agreement between the expected scaling relations and the model.

Finally, for intermediate driving frequencies, we already approximated the oscillation amplitude [Eq. (7)] by neglecting viscous friction and presuming constant contact between colloid and network. Consequently, we can estimate the steady-state cavity volume using the same set of approximations by setting $|\dot{X}| \approx 2A_{\text{intermediate}}/(\pi/\Omega)$ in Eq. (5). This yields

$$V_{\text{intermediate}} = \frac{\Omega}{\pi}\frac{\Omega \sin\left(\frac{2\pi\Omega_0}{\Omega+\Omega_0}\right) - \Omega_0 \sin\left(\frac{2\pi\Omega}{\Omega+\Omega_0}\right)}{\Omega^2\Omega_0 - \Omega_0^3}, \qquad (8)$$

which is indicated by the dotted red line in the inset of Fig. 2(d). The agreement with the full model is again good for the used parameter values.

This establishes the general behavior of the expanding cavity. We now investigate the effect of varying model parameters.

VI. VARYING MODEL PARAMETERS

The key parameters of interest are the (scaled) natural frequency of the network, Ω_0, closely related to the elastic modulus and cross-linking density, and the (scaled) damping ratio, B. Figure 3(a) shows the steady-state oscillation amplitude as a function of the driving frequency, for $\Omega_0 = 0.1$ (silver curve), 1.0 (grey curve), and 10.0 (black curve). All curves correspond to the same damping ratio $B = 0.05$. Here, we have taken care to scale the amplitude $A\Omega_0^2$ and the driving frequency Ω/Ω_0, such that the different lines collapse onto a single curve in the low- and high-frequency limits. This already implies that the position of the resonance can be shifted by varying Ω_0 and that, similarly, its amplitude scales inversely with Ω_0. That is, a greater elastic modulus both speeds up the oscillation, and suppresses its amplitude. Any additional features apparent from Fig. 3(a) are superimposed on top of this dominating trend.

In particular, the inset of Fig. 3(a) shows that the behavior of the resonance peak itself is more subtle than our introduced scaling implies: here the different curves do not overlap. As it turns out, the magnitude of this peak depends more strongly on Ω_0 than the $\propto \Omega_0^{-2}$ dependence predicted by the theoretical estimate of Eq. (7), which is shown in the inset by the dotted red curve. This dependence is already absorbed into the chosen scaling. Although the qualitative agreement with all curves is reasonable, this estimate only *quantitatively* describes the grey curve, which corresponds to the (scaled) natural frequency $\Omega_0 = t_R\sqrt{k/m} = 1.0$. In other words, our theoretical estimate for the resonance is quantitative if the natural timescale of the oscillation, $\sqrt{k/m}$, is comparable to the relaxation time of the polymer gel, t_R, and becomes qualitative if one grows much larger than the other.

The above suggests that the assumptions we make in deriving Eq. (7) break down for exceedingly weak or strong elastic moduli. For the former, the elastic restoring force no longer dominates the viscous friction with the background fluid, which in turn slows down the colloid and diminishes the amplitude of the oscillation more than predicted theoretically. For the latter, the elastic restoring force is sufficiently strong such that the colloid does not leave the initial turning points of its oscillation with negligible residual velocity. Instead, the oscillation grows in amplitude over the first few periods before settling to a steady state. As a result, the theoretical estimate underestimates the steady-state amplitude in this case.

In a similar vein, Fig. 3(b) shows the concomitant cavity volume in the steady state. Here, we employ the same scaling

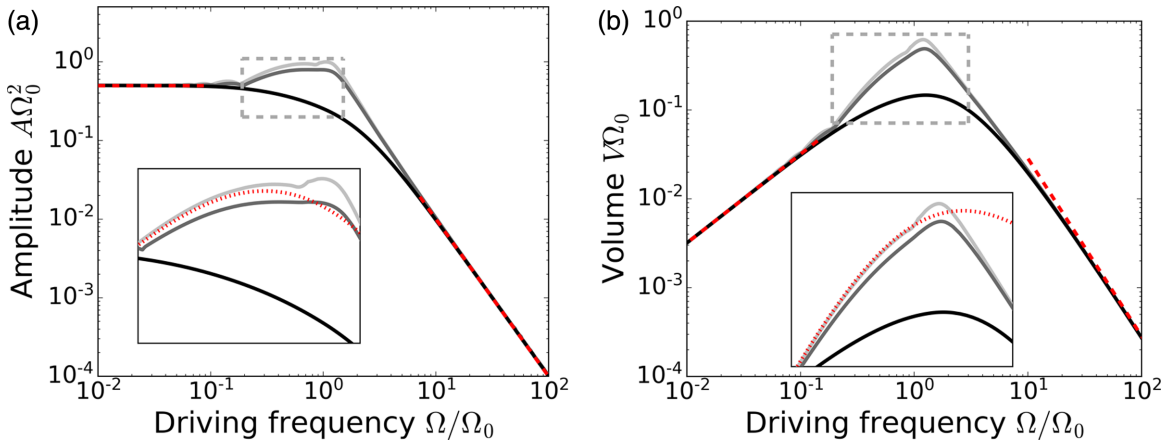

FIG. 4. Scaled steady-state amplitude A of the colloid oscillation (left) and the corresponding cavity free volume V (right) as a function of the scaled driving frequency Ω, on logarithmic scale. The curves correspond to $B = 0.01$ (silver), 0.1 (grey), and 1.0 (black), all for $\Omega_0 = 0.7$. The dashed red lines denote low- and high-frequency scaling laws. The zoomed-in inset is indicated in grey; the dotted red curves in the insets correspond to the theoretical estimates of Eq. (7) (left) and Eq. (8) (right), respectively.

for the driving frequency, Ω/Ω_0, but scale the cavity volume $V\Omega_0$. This ensures universal behavior at low driving frequencies, in good correspondence with the relevant scaling law, shown by the dashed red line. The same universality applies to the theoretical estimate of Eq. (8), which the chosen scaling renders independent of Ω_0, such that the dotted red curve shown in the inset applies to all of the plotted curves. In contrast, the plotted curves differ by a factor Ω_0 in the high-frequency limit, although they scale identically with Ω. This cannot be scaled out without giving up the universality at low and intermediate frequencies. Consequently, we again find that, first and foremost, increasing Ω_0 shifts the resonance, and suppresses the generation of free volume in the low- and intermediate frequency regimes. This effect vanishes in the high-frequency limit, which is dominated by inertial effects.

Looking beyond these features, which are absorbed into the chosen scaling, the more subtle effects of varying the network's natural frequency can once again be found around the system's resonance. One trend that is apparent from comparing Figs. 3(a) and 3(b) is that the resonance of the cavity free volume is shifted to higher driving frequencies relative to that of the oscillation amplitude. This stems from the cavity relaxing viscoelastically as a function of time, which biases the results, both in magnitude and in position, toward faster actuation. This effect becomes more pronounced if the natural timescale of the oscillation, $\sqrt{m/k}$, is large relative to the relaxation time of the polymer gel, t_R. Hence the effect is most apparent from the silver curve, corresponding to $\Omega_0 = t_R\sqrt{k/m} = 0.1$.

Following this, the effect of varying the damping ratio, i.e., the friction coefficient of the viscoelastic medium in which the colloid is embedded, follows a very similar trend, as Fig. 4 shows. Here, the different curves correspond to $B = 0.01$ (black), 0.1 (grey), and 1.0 (silver), and we set $\Omega_0 = 0.7$. Since the value of B has no effect on the scaling laws and theoretical estimates we use, varying the damping ratio *solely* affects the form of the resonance peak, as highlighted by the insets. First and foremost, we see that the resonance in terms of both amplitude [Fig. 4(a)] and cavity volume [Fig. 4(b)] is suppressed upon increasing the damping ratio, as expected. Perhaps more interestingly, we find that for small values of the damping ratio, where the theoretical estimates of Eqs. (7) and (8) are most suitable, the resonance peak splits in two. We expect that this stems from the interplay between purely elastic interactions and the external field, since increasing B suppresses this split. The same is true for the finer model features apparent in the low-frequency regime, which are, like the split resonance peak, discussed in Appendices B and C.

VII. CONCLUSION

In summary, we have investigated the dynamics of a driven colloid embedded in a cross-linked polymer gel, immersed in a viscous background fluid, as a mechanism for rendering such materials responsive. Through a relatively simple, yet nontrivial, model derived from the harmonic oscillator, we show that the oscillatory motion of the colloid can induce a microscopic cavity of a size far exceeding the length scale of the colloid in the steady state. As a function of the driving frequency, we find that the oscillation is well described by simple scaling laws in the low- and high-frequency limits, and we propose closed-form theoretical estimates to describe the resonance that occurs at intermediate frequencies. These estimates qualitatively describe the dependence of the resonance on model parameters, and become quantitative for strongly underdamped systems.

In particular, we conclude that the model dynamics is primarily governed by an interplay between the elastic properties of the network and the external field, with the local friction mainly having a suppressing effect. Specifically, we report that increasing the elastic restoring force acting throughout the network, accessible through the gel's elastic modulus or cross-link density, increases the resonant driving frequency, and diminishes the resonant amplitude and steady-state cavity volume for low and intermediate frequencies; this effect vanishes in the high-frequency limit. Finally, the model also exhibits a variety of finer features, which we rationalize in the Appendix by considering various simplifying assumptions.

Our work provides a proof of concept for effecting local free-volume generation, and with it responsivity, in cross-linked polymer gels. We note, however, that the same model considerations could be tailored to describe polymer melts. In that case, there is no longer a direct link between the viscosity of the background fluid and the friction coefficient, which then instead derives from the melt itself behaving like a liquid on long timescales.

Although in this paper we focused on the oscillation of a single colloidal particle embedded in a cross-linked polymer gel, we expect our main findings to also be applicable to larger numbers. This is because we expect at least a linear superposition of the individual responses, possibly amplified by their mutual interactions mediated by the polymer network [61]. Such an amplification can be explored further by considering shrewdly placing the colloids, e.g., on a lattice, rather than dispersing them randomly in the gel. Regardless of placement, the interactions should be relevant even for relatively small colloid densities, e.g., on length scales far exceeding the cross-link spacing, since such network-mediated interactions decay algebraically in space as $1/r$. Thus our approach can be interpreted as a lower bound for such systems, in which we effectively describe a small volume element of the material in which a single colloid is embedded, and disregard possible network-mediated interactions. This presents a first step toward rendering arbitrary cross-linked polymer networks suitable for, e.g., self-cleaning purposes, pattern formation, and transport of molecular cargo.

Importantly, our findings can be directly verified through experiments or computer simulations by embedding colloidal particles into a dense, cross-linked polymer network or melt during the synthesis. If the colloids are provided with a sufficiently strong coupling to the external field of choice, e.g., electric, we expect oscillatory actuation to give rise to appreciable changes in volume and porosity. This claim is supported qualitatively by recent viscosity experiments on aqueous solutions of polyethylene glycol [29], where a quartz tuning fork oscillating at nanoscopic amplitudes demonstrates significant free-volume generation.

The same is true for the liquid crystal networks discussed in the introduction, where reorientation or cis-to-trans isomerization of rodlike molecules gives rise to the free-volume generation. Our findings suggest that the expansion reported for these materials upon actuation need not be inherently linked to the molecules being grafted to the polymer network [31,33] but can instead follow purely from reorientation inside the polymer matrix. This puts our work in broader perspective.

Finally, a possible extension of our work concerns the assumption of plastic rearrangements occurring in the cross-linked polymer gel. In this work, we assumed, for the sake of simplicity, that both elastic relaxation and plastic rearrangements occur on the same timescales. It would be interesting, however, to probe how varying the timescale corresponding to plastic rearrangements, which we expect to be slower than that of elastic relaxation in practice, influences the steady state. Specifically, such an extension may render the model, and in particular the steady state it predicts, less sensitive to the transient stages of dynamics.

ACKNOWLEDGMENTS

This research received funding from the Dutch Research Council (NWO) in the framework of the ENW PPP Fund for the top sectors and from the Ministry of Economic Affairs in the framework of the "PPS-Toeslagregeling."

APPENDIX A: SELECTIVE FRICTION

In writing the dynamical equations (1)–(6) in the main text we assume that the polymer network does not screen the viscous friction of the colloid with the background fluid. Here, we investigate the effects of relaxing this assumption and instead considering a friction coefficient that explicitly depends on whether the colloid is in contact with the cavity wall or not. To this end, we rewrite our governing set of equations, Eq. (6) in the main text, as

$$\begin{cases} \ddot{X} + 2B\dot{X}[1-(1-\varphi)\delta_{\text{front contact}}] + \Omega_0^2(X-X_0)(\delta_{\text{front contact}}+\delta_{\text{rear contact}}) = \sin\Omega\tau, \\ \dot{V} = |\dot{X}|\,\delta_{\text{front contact}} - V. \end{cases} \tag{A1}$$

Here, we have replaced the contact function used in the main text, δ_{contact}, by two functions: $\delta_{\text{front contact}}$ and $\delta_{\text{rear contact}}$. The former applies if the velocity of the colloid is directed toward the cavity wall it is in contact with, whereas the latter applies if the velocity of the colloid is directed away from said wall. This distinction allows us to *only* adapt the friction coefficient if the colloid is moving into the polymer network, and not if it is moving away from it. In addition, we have recast the viscous term using a factor $1-\varphi$, which we use to compare the cases of complete screening ($\varphi = 0$), no screening ($\varphi = 1$), and reinforced friction ($\varphi = 2$). The steady-state oscillation amplitude and cavity volume corresponding to these cases are represented in Fig. 5 by the solid, dashed, and dotted curves, respectively. For this, we use the same parameter values as in the main text, $\Omega_0 = 0.7$ and $B = 0.05$.

From the figure we find that the general trends of our clear scaling laws in the low- and high-frequency limits, with a pronounced resonance at intermediate frequencies (theoretical estimates not shown here), persist upon relaxing the assumption of complete screening. The decrease in resonant amplitude upon increasing φ is expected, as this effectively makes the role of viscous friction more significant. In correspondence with out findings in the main text, this does not change the scaling laws in the low- and high-frequency limits.

In addition, we see that the finer features of the model, such as the resonance peak being split in two and the emergence of multiple local optima in the low-frequency regime, are sup-

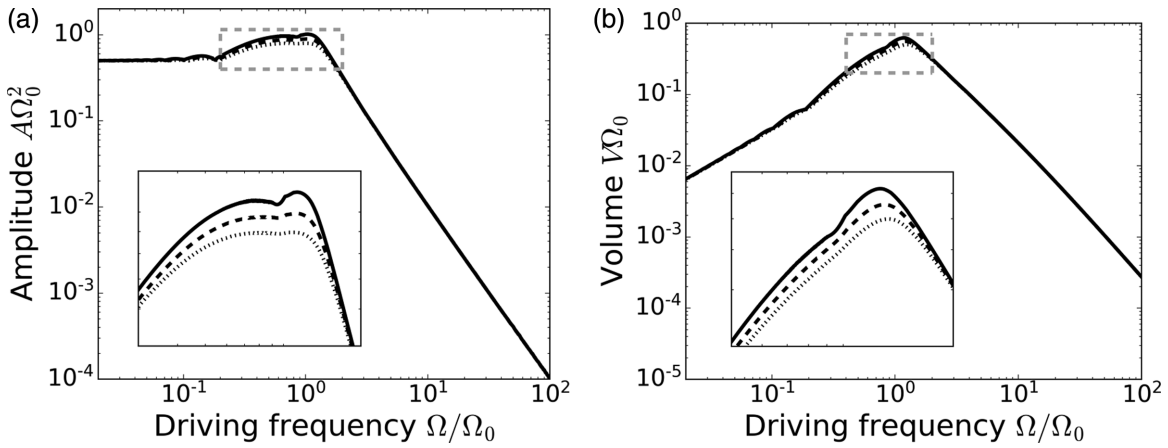

FIG. 5. Scaled steady-state amplitude A of the colloid oscillation (left) and the corresponding cavity volume V (right) as a function of the scaled driving frequency Ω, on logarithmic scale. The different curves correspond to $\varphi = 0$ (solid), 1 (dashed), and 2 (dotted). The zoomed-in inset is indicated in grey. Parameter values used: $\Omega_0 = 0.7$ and $B = 0.05$.

pressed upon increasing φ. This is likewise in line with what we reported in the main text upon varying the damping ratio B, and so supports the qualitative picture sketched above. That is, rendering viscous friction nonselective, or even modeling reinforced friction, does not fundamentally change the model features but can be interpreted in a similar vein as tuning the system's viscosity.

APPENDIX B: COLLOID DYNAMICS: FINE FEATURES

Figure 6 presents an analog of Fig. 2 in the main text, with the finer model features numbered one through six. For the sake of illustration, here we set $\varphi = 0$, which renders the finer model features more pronounced without fundamentally altering them.

We start by investigating the points indicated in Fig. 6(a), which shows the steady-state oscillation amplitude. The first point of interest corresponds to a driving frequency $\Omega = 3.0$, which significantly exceeds the natural frequency of the network, $\Omega_0 = 0.7$. The first panel of Fig. 7 shows the corresponding colloid oscillation, from which a competition between the driving frequency (individual oscillations) and the network's natural frequency (enveloping oscillation) is clear. The significant mismatch between the two results in an oscillation that settles to a modest amplitude in line with the high-frequency scaling relation discussed in the main text.

Following this, the second point of interest in Fig. 6(a) corresponds to a local maximum in amplitude, at $\Omega = 0.73$; the inset more clearly displays this feature. This marks the first of multiple resonant driving frequencies, which in this case tunes into the natural frequency of the network to rapidly achieve a steady-state oscillation, as illustrated by the second panel of Fig. 7.

If we further decrease the driving frequency we find a dip in the oscillation amplitude in Fig. 6(a). The onset of this dip roughly coincides with the network's natural frequency, since for $\Omega < \Omega_0$ the turning point of the oscillation occurs before

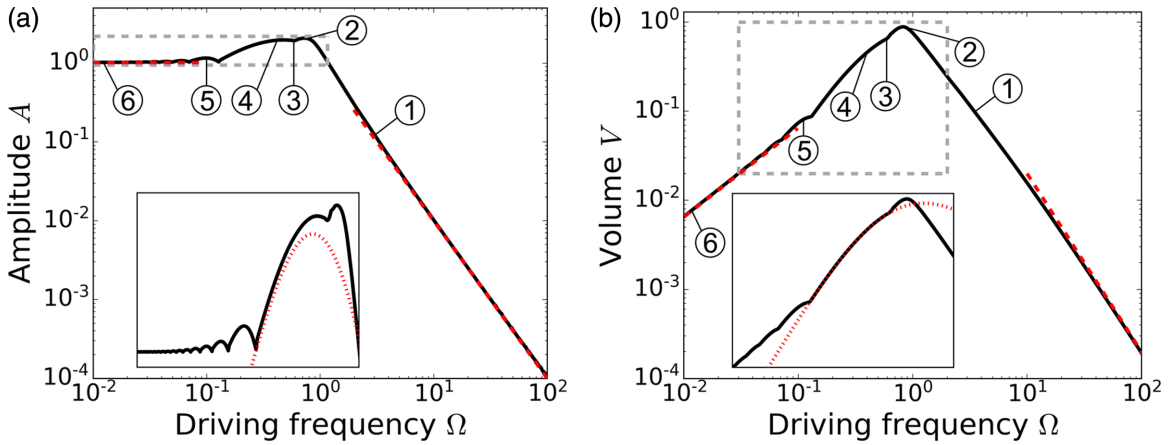

FIG. 6. Scaled steady-state amplitude A of the colloid oscillation (left) and the corresponding cavity volume V (right) as a function of the scaled driving frequency Ω, on logarithmic scale. The dashed red lines denote the low- and high-frequency scaling laws explained in the main text and we use the numbers (1) through (6) to indicate points of interest in the diagram. The zoomed-in inset is indicated in grey; the dotted red curves in the insets correspond to the theoretical estimates of Eq. (7) (left) and Eq. (8) (right) in the main text, respectively. Parameter values used: $\Omega_0 = 0.5$, $B = 0.1$.

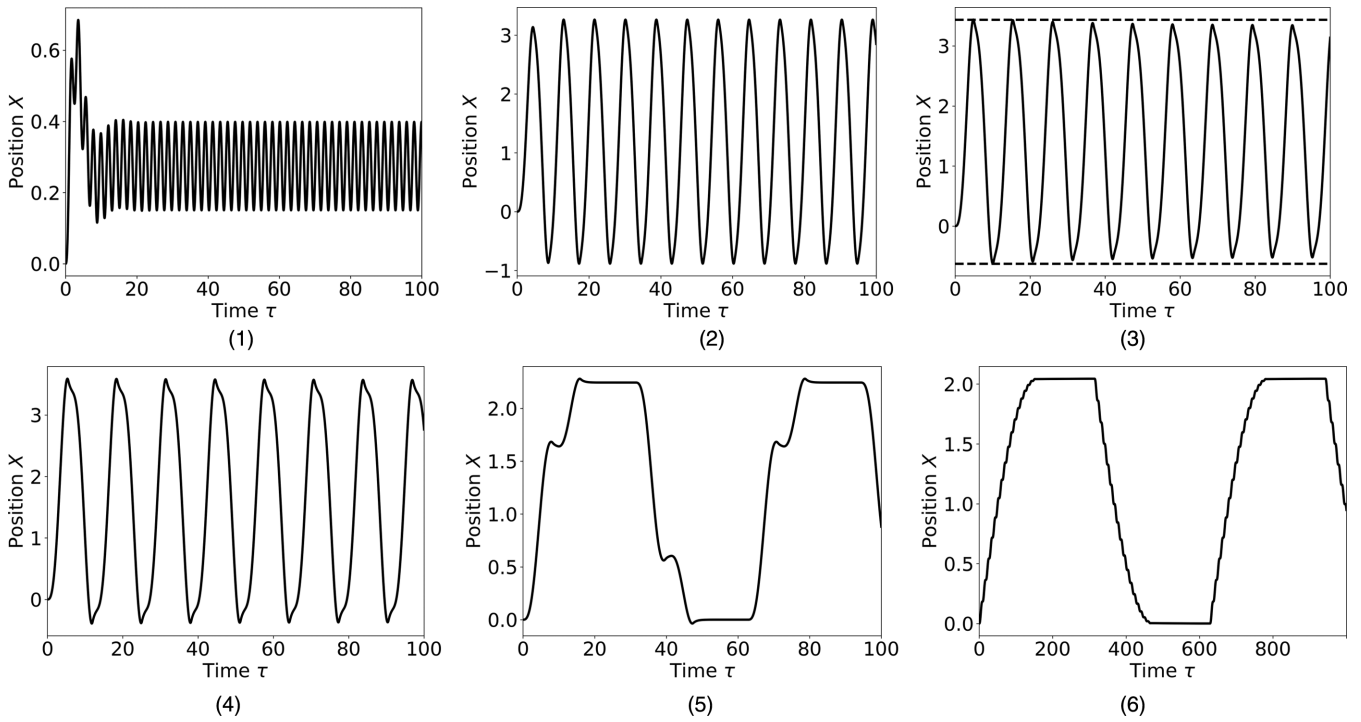

FIG. 7. Scaled colloid position X as a function of the scaled time τ. (1) through (6) correspond to the scaled driving frequencies $\Omega =$ 3.0, 0.73, 0.59, 0.48, 0.10, and 0.010, respectively in Fig. 2. Parameter values used: $\Omega_0 = 0.7$, $B = 0.05$.

the applied field changes sign. This means that the colloid is briefly slowed down by the applied field after turning, suppressing the oscillation amplitude. This is shown by the third panel of Fig. 7, which corresponds to the dip minimum, at $\Omega = 0.59$. From the figure, it is apparent that the oscillation amplitude decays as a function of time, as can be seen by comparing with the dashed black lines that show the initial amplitude. The reason the dip in the resonance curve does not extend further is because for sufficiently low driving frequencies the field repeatedly pushes the colloid back into the cavity wall, which in turn pushes back. In that case, the elastic restoring force compensates the field-induced slowing-down effect.

Upon decreasing the driving frequency further still, we discover a second resonant driving frequency, $\Omega = 0.48$, which marks the fourth point of interest in Fig. 6(a). The inset shows that this resonance corresponds well with the theoretical estimate of Eq. (7) in the main text (dotted red line), suggesting the assumptions of constant contact prior to the turning point and negligible residual velocity and acceleration at the turning point are justified in this regime. It then follows that this resonance coincides with the driving frequency that maximizes the position of the first turning point, as the oscillation continues identically from the point onward.

If we look at the inset of Fig. 6(a) for even lower driving frequencies, we find that an array of resonances steadily decreasing in magnitude emerges. The first of these peaks corresponds to the fifth point of interest, which no longer lies on the dotted red line of Eq. (7) in the main text. This is because for driving frequencies that are sufficiently slow compared to the network's natural frequency, the colloid undergoes multiple minor oscillations (on the network's natural timescale) before reaching its eventual turning point. The fifth panel in Fig. 7 illustrates this feature, which is not specific to our model but can be derived identically from a simple, driven harmonic oscillator.

Based on the above, it should come as no surprise that subsequent, smaller peaks in Fig. 6(a), at even lower driving frequencies, correspond to an increasing number of these minor oscillations, $n = 1, 2, 3, \ldots$ The onset of these peaks follow the higher-order harmonics $\Omega = \Omega_0/(1 + 4n)$. Finally, in the low-frequency limit, the trajectory of the colloid approaches a continuous curve, as shown in the sixth panel of Fig. 7, which agrees well with the low-frequency scaling relation discussed above.

This concludes the discussion of the colloid dynamics, from which we find that many of the finer model features can only be understood by considering the full dynamics, rather than solely the steady-state amplitude; this does not alter our message in the main text, however. Next, we discuss the fine features apparent from the concomitant volume expansion of the microscopic cavity.

APPENDIX C: CAVITY EXPANSION: FINE FEATURES

The finer features superimposed on the steady-state cavity free volume resonance curve, as indicated by the numbered points in Fig. 6(b), follow the same trends as discussed in Sec. B. That is, for high driving frequencies [point (1)] the mismatch between driving and natural frequency leads to an erratic expansion of the microscopic cavity before it settles on its steady state, as the first panel of Fig. 8 shows. We reiterate that the frequency with which the cavity volume oscillates is twice that of the colloid oscillation, as the cavity volume is expanded upon both leftward and rightward motion.

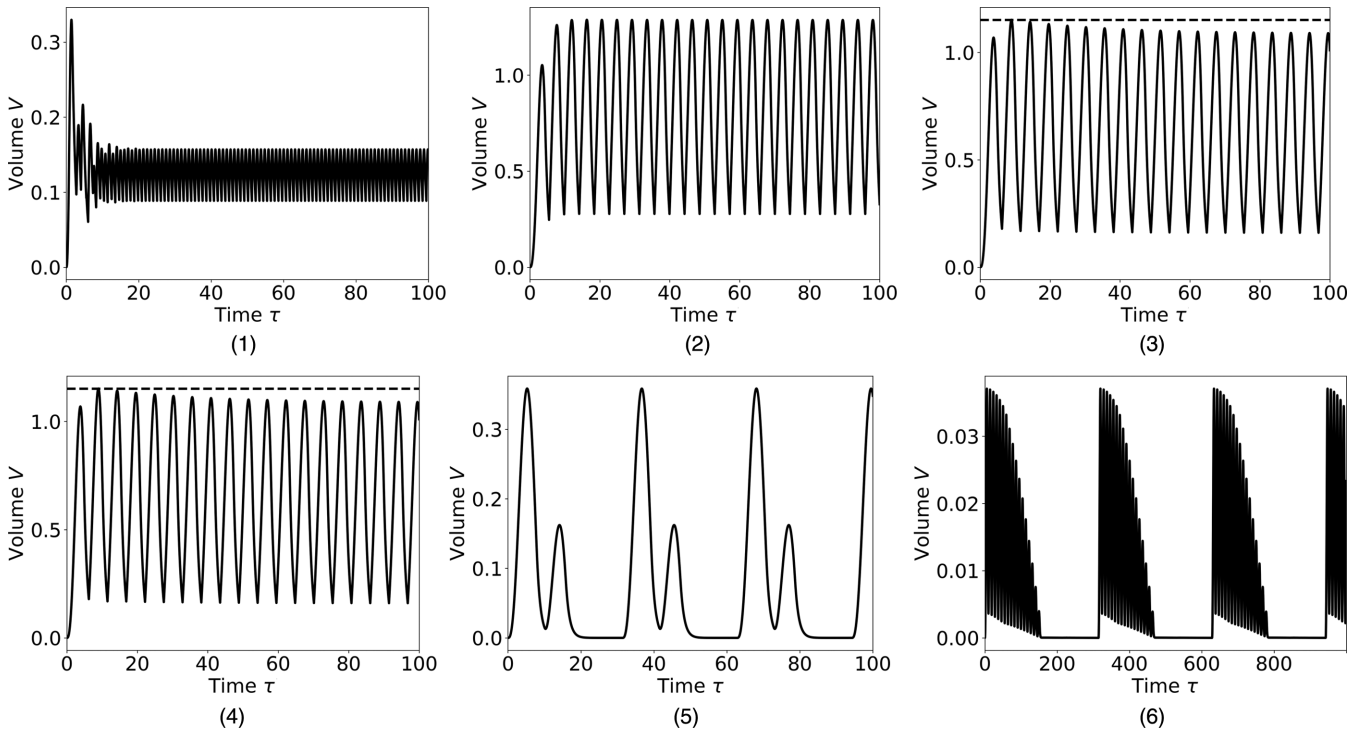

FIG. 8. Scaled cavity volume V as a function of the scaled time τ. (1) through (6) correspond to the scaled driving frequencies $\Omega = 3.0,\ 0.73,\ 0.59,\ 0.48,\ 0.10,$ and 0.010, respectively [see Fig. 6(b)]. Parameter values used: $\Omega_0 = 0.7$, $B = 0.05$.

Following this, the primary resonance in terms of volume expansion is located at the same driving frequency as the highest-frequency resonance discussed in Sec. B (point 2). This is not surprising, as the viscoelastic relaxation of the cavity biases the results toward faster actuation. The second panel of Fig. 8 shows the corresponding expansion of the cavity volume.

Next, point 3 coincides with the dip that separates the two major resonance peaks of the model. In Sec. B, we argued that this results from to the incommensurability of the driving frequency and the network's natural frequency. The third panel of Fig. 8 shows the corresponding cavity volume, which decays in a manner similar to the colloid position in the third panel of Fig. 7.

Point 4 then marks the second resonance of the system, which is well described by the theoretical estimate of Sec. C [see the inset of Fig. 6(b)]. The fourth panel of Fig. 8 shows the corresponding evolution of the cavity volume, which does not exhibit the distinct decay as a function of time we discussed above.

Finally, the low-frequency limit is again characterized by the colloid undergoing multiple minor oscillations on top of the one imposed by the driving force. The fifth panel of Fig. 8 indicates that if the colloid undergoes only one such oscillation, the expansion of the cavity volume splits in two distinct stages: before and after. This is because at the point of the minor oscillation the colloid's motion is almost completely arrested, and so the cavity volume relaxes.

The sixth panel of Fig. 8 illustrates how this feature generalizes to many minor oscillations, in which case the cavity volume approaches a continuous curve. The resonance peaks corresponding to these features in Fig. 6(b) are much less pronounced than for the oscillation amplitude due to the viscoelastic relaxation of the gel.

APPENDIX D: EXTERNAL FIELD: SINE VERSUS COSINE

As discussed in the main text, the fact that we allow plastic rearrangements to occur causes the eventual steady state to depend nontrivially on the transient stages of dynamics. This is because in these stages plastic rearrangements occur. Accordingly, driving the colloid with an external field in the form of a cosine yields distinct results from actuation by a sine field, since the initial "kick" provided by the former can have a large effect on which plastic rearrangements occur. Figure 9 compares the steady states achieved by an external field in the form of a sine (grey curve) and an external field in the form of a cosine (black curve). Here we use $\varphi = 0$, as in the main text.

The most distinctive feature apparent from Fig. 9(a) is that the black curve (cosine actuation) lies markedly lower than the grey curve (sine actuation) in the low-frequency limit. This is because the initial "kick" provided by the cosine external field immediately induces significant plastic rearrangements. In essence, this translates the colloid to a new rest position, from which slower oscillations, like those induced by a sine external field, can subsequently take place. The key difference, however, is that this new rest position is not stress free, since elastic stresses were incurred when the colloid displaced the cross-linked polymer gel to this new reference configuration. These stresses only relax once the external field varies sufficiently to force the colloid away from its new

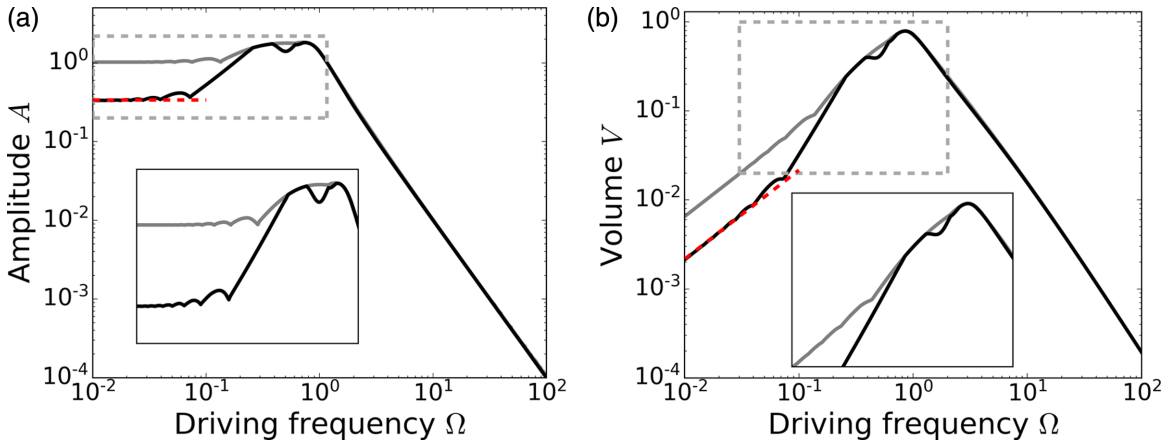

FIG. 9. Scaled steady-state amplitude A of the colloid oscillation (left) and the corresponding cavity volume V (right) as a function of the scaled driving frequency Ω, on logarithmic scale. The different curves correspond to an external field $\sin \Omega\tau$ (grey) and an external field $\cos \Omega\tau$ (black). The dashed red lines denote the low-frequency scaling laws discussed in the text and the zoomed-in inset is indicated in grey. Parameter values used: $\Omega_0 = 0.7$ and $B = 0.05$.

reference configuration. Since any ensuing oscillation must occur against the backdrop of these residual stresses, their corresponding amplitude becomes smaller.

Mathematically, turning on a cosine external field initiates a swift translation on the network's natural timescale, $1/\Omega_0$. In this case, inertia cannot be neglected. Instead ignoring viscous friction, and approximating $\cos \Omega\tau \approx 1$, we find

$$X(\tau) = \frac{1}{\Omega_0^2}(1 - \cos \Omega_0 \tau). \tag{D1}$$

The colloid follows this trajectory during its initial oscillation, freeing up a cavity of unoccupied volume in its wake. The model states that this cavity shrinks exponentially via plastic rearrangements. Subsequently, the motion of the colloid is arrested if, after passing the turning point of its oscillation, it encounters the cavity wall that is closing in due to plastic rearrangements. By using the dynamical equation for the cavity volume, we estimate this to occur at

$$X_0 = \frac{2}{\Omega_0^2} - \frac{1}{2}\frac{1 + e^{-\pi/\Omega_0}}{1 + \Omega_0^2}. \tag{D2}$$

Since we assume plastic rearrangements, the colloid maintains the rest position estimated above until the external field changes direction and forces it away. In the low-frequency limit, this process occurs gradually, justifying us neglecting inertia and friction henceforth. Following the line of reasoning put forth in the main text, a balance of the elastic force and and the external field then suggests that the colloid is perturbed from its rest position by $|X - X_0| = 1/\Omega_0^2$. Since the rest positions of the cavity walls are given by $X_0 = 0$ and Eq. (D2), respectively, the steady-state amplitude becomes $A_{\text{low}} = \frac{1}{2}(1 + e^{-\pi/\Omega_0})/(1 + \Omega_0^2)$, in good correspondence with Fig. 9(a) (dashed red line).

Comparing with Fig. 9(b) shows that the same discrepancy holds for the steady-state cavity free volume in the low-frequency limit. In the main text, we already argued that in this regime we expect the free volume generated by colloid motion to be exactly compensated by the viscoelastic relaxation of the polymer gel in the steady state. Thus, using the estimate for the steady-state amplitude derived above, we find $V_{\text{low}} = \frac{\Omega}{\pi}(1 + e^{-\pi/\Omega_0})/(1 + \Omega_0^2)$, in good correspondence with Fig. 9(b) (dashed red line).

Figure 9 shows that the discrepancy between the grey and the black curves shrinks as we increase the driving frequency and finally vanishes completely in the high-frequency limit. This is because the main feature distinguishing the two is the initial "kick" provided by the cosine external field, and the concomitant plastic rearrangements. As the oscillation of the external field is increased this effect becomes increasingly minor, becoming negligible for sufficiently high driving frequencies.

The final feature distinguishing the black curve (cosine actuation) from the grey curve (sine actuation) in both panels of Fig. 9 is that the dip splitting the resonance into two peaks is significantly more pronounced. This indicates that also the fine model features can be altered nontrivially by the plastic rearrangements that occur during the transient stages of actuation, though which features occur remains unchanged.

[1] W. C. Poon and D. Andelman, *Soft Condensed Matter Physics in Molecular and Cell Biology* (CRC Press, Boca Raton, FL, 2006).

[2] G. H. Wadhams and J. P. Armitage, Nat. Rev. Mol. Cell Biol. **5**, 1024 (2004).

[3] R. Elbaum, L. Zaltzman, I. Burgert, and P. Fratzl, Science **316**, 884 (2007).

[4] E. Reyssat and L. Mahadevan, J. R. Soc. Interface **6**, 951 (2009).

[5] M. A. C. Stuart, W. T. Huck, J. Genzer, M. Müller, C. Ober, M. Stamm, G. B. Sukhorukov, I. Szleifer, V. V. Tsukruk, M. Urban *et al.*, Nat. Mater. **9**, 101 (2010).

[6] D. Roy, J. N. Cambre, and B. S. Sumerlin, Prog. Polym. Sci. **35**, 278 (2010).

[7] M. Wei, Y. Gao, X. Li, and M. J. Serpe, Polym. Chem. **8**, 127 (2017).
[8] A. Bratek-Skicki, Appl. Surf. Sci. Adv. **4**, 100068 (2021).
[9] G. Chen and A. S. Hoffman, Nature (London) **373**, 49 (1995).
[10] D. Schmaljohann, Adv. Drug Deliver. Rev. **58**, 1655 (2006).
[11] S. Murdan, J. Control. Release **92**, 1 (2003).
[12] T. Manouras and M. Vamvakaki, Polym. Chem. **8**, 74 (2017).
[13] F. Ercole, T. P. Davis, and R. A. Evans, Polym. Chem. **1**, 37 (2010).
[14] J.-F. Gohy and Y. Zhao, Chem. Soc. Rev. **42**, 7117 (2013).
[15] Y. Qiu and K. Park, Adv. Drug Deliver Rev. **53**, 321 (2001).
[16] P. Gupta, K. Vermani, and S. Garg, Drug Discov. Today **7**, 569 (2002).
[17] R. A. Stile and K. E. Healy, Biomacromolecules **2**, 185 (2001).
[18] S. Miao, N. Castro, M. Nowicki, L. Xia, H. Cui, X. Zhou, W. Zhu, S.-j. Lee, K. Sarkar, G. Vozzi *et al.*, Mater. Today **20**, 577 (2017).
[19] R. Shankar, T. K. Ghosh, and R. J. Spontak, Soft Matter **3**, 1116 (2007).
[20] D. Morales, E. Palleau, M. D. Dickey, and O. D. Velev, Soft Matter **10**, 1337 (2014).
[21] S. M. Mirvakili and I. W. Hunter, Adv. Mater. **30**, 1704407 (2018).
[22] L. Montero de Espinosa, W. Meesorn, D. Moatsou, and C. Weder, Chem. Rev. **117**, 12851 (2017).
[23] E. G. Bellomo, M. D. Wyrsta, L. Pakstis, D. J. Pochan, and T. J. Deming, Nat. Mater. **3**, 244 (2004).
[24] B. Xin and J. Hao, Chem. Soc. Rev. **39**, 769 (2010).
[25] L. F. Boesel, C. Greiner, E. Arzt, and A. Del Campo, Adv. Mater. **22**, 2125 (2010).
[26] R. Weeber, S. Kantorovich, and C. Holm, Soft Matter **8**, 9923 (2012).
[27] S. Kondaveeti, A. T. S. Semeano, D. R. Cornejo, H. Ulrich, and D. F. S. Petri, Colloid. Surface B **167**, 415 (2018).
[28] S. Ganguly and S. Margel, Polymers-Basel **13**, 4259 (2021).
[29] K. Sozanski, A. Wisniewska, T. Piasecki, K. Waszczuk, A. Ochab-Marcinek, T. Gotszalk, and R. Holyst, Soft Matter **10**, 7762 (2014).
[30] H. Finkelmann, H.-J. Kock, and G. Rehage, Makromol. Chem., Rapid Commun. **2**, 317 (1981).
[31] D. Liu, N. B. Tito, and D. J. Broer, Nat. Commun. **8**, 1526 (2017).
[32] D. Liu and D. J. Broer, Nat. Commun. **6**, 8334 (2015).
[33] A. H. Gelebart, D. Liu, D. J. Mulder, K. H. J. Leunissen, J. van Gerven, A. P. H. J. Schenning, and D. J. Broer, Adv. Funct. Mater. **28**, 1705942 (2018).
[34] D. Liu, L. Liu, P. R. Onck, and D. J. Broer, Proc. Natl. Acad. Sci. USA **112**, 3880 (2015).
[35] D. Liu, C. W. Bastiaansen, J. M. den Toonder, and D. J. Broer, Angew. Chem. Int. Ed. **51**, 892 (2012).
[36] M. E. McConney, A. Martinez, V. P. Tondiglia, K. M. Lee, D. Langley, I. I. Smalyukh, and T. J. White, Adv. Mater. **25**, 5880 (2013).
[37] G. Babakhanova, A. P. Schenning, D. J. Broer, and O. D. Lavrentovich, in *Emerging Liquid Crystal Technologies XIV* (SPIE, 2019), Vol. 10941, p. 109410I.
[38] H. M. van der Kooij, S. A. Semerdzhiev, J. Buijs, D. J. Broer, D. Liu, and J. Sprakel, Nat. Commun. **10**, 3501 (2019).
[39] H. M. van der Kooij, D. J. Broer, D. Liu, and J. Sprakel, ACS Appl. Mater. Interfaces **12**, 19927 (2020).
[40] A. Cao, R. J. van Raak, X. Pan, and D. J. Broer, Adv. Funct. Mater. **29**, 1900857 (2019).
[41] Y. Zhan, W. Zhang, A. Özden, S. Houben, M. Schuster, H. Gojzewski, G. Zhou, D. J. Broer, and D. Liu, ACS Appl. Polym. Mater. **2**, 4071 (2020).
[42] R. N. Zia, Annu. Rev. Fluid Mech. **50**, 371 (2018).
[43] G. Batchelor, J. Fluid Mech. **41**, 545 (1970).
[44] G. Batchelor, J. Fluid Mech. **119**, 379 (1982).
[45] G. Batchelor and C.-S. Wen, J. Fluid Mech. **124**, 495 (1982).
[46] T. M. Squires and J. F. Brady, Phys. Fluids **17**, 073101 (2005).
[47] A. S. Khair and J. F. Brady, J. Fluid Mech. **557**, 73 (2006).
[48] R. N. Zia and J. F. Brady, J. Fluid Mech. **658**, 188 (2010).
[49] N. J. Hoh and R. N. Zia, J. Fluid Mech. **785**, 189 (2015).
[50] H. C. Chu and R. N. Zia, J. Rheol. **60**, 755 (2016).
[51] T. Odijk, Physica A **337**, 389 (2004).
[52] Y. He, L. Li, T. Taniguchi, R. Tuinier, and T.-H. Fan, Phys. Rev. Fluids **5**, 013302 (2020).
[53] T. Odijk, Macromolecules **29**, 1842 (1996).
[54] T. Odijk, Biophys. J. **79**, 2314 (2000).
[55] R. Tuinier, J. K. G. Dhont, and T.-H. Fan, Europhys. Lett. **75**, 929 (2006).
[56] T.-H. Fan, J. K. G. Dhont, and R. Tuinier, Phys. Rev. E **75**, 011803 (2007).
[57] T. Kalwarczyk, K. Sozanski, A. Ochab-Marcinek, J. Szymanski, M. Tabaka, S. Hou, and R. Holyst, Adv. Colloid Interface Sci. **223**, 55 (2015).
[58] P. E. Rouse Jr., J. Chem. Phys. **21**, 1272 (1953).
[59] R. R. Kumal, T. E. Karam, and L. H. Haber, J. Phys. Chem. C **119**, 16200 (2015).
[60] G. West, Polymer **10**, 751 (1969).
[61] L. Di Michele, A. Zaccone, and E. Eiser, Proc. Natl. Acad. Sci. USA **109**, 10187 (2012).